# A Flight Control Approach for Small Reentry Vehicles

Tim Bevacqua*, Tony Adami†, J. Jim Zhu‡
School of Electrical Engineering and Computer Science
Avionics Engineering Center, Ohio University
Athens, OH 45710

Prabhakara P. Rao§
Lockheed Martin Space Systems
Denver, CO 80201

**Abstract**

Flight control of small crew return vehicles during atmospheric reentry will be an important technology in any human space flight missions undertaken in the future. The control system presented in this paper is applicable to small crew return vehicles in which reaction control system (RCS) thrusters are the only actuators available for attitude control. The control system consists of two modules: (i) the attitude controller using the trajectory linearization control (TLC) technique, and (ii) the reaction control system (RCS) control allocation module using a dynamic table-lookup technique. This paper describes the design and implementation of the TLC attitude control and the dynamic table-lookup RCS control allocation for nominal flight along with design verification test results.

## 1. INTRODUCTION

One of the goals of the NASA Orbital Space Plane (OSP) program was to provide a small crew transfer vehicle for the International Space Station, using only technology which had already been matured to a level suitable for human flight. Two concept vehicles proposed to meet this challenge were a small winged lifting-body (WLB), and an axial-symmetric capsule (ASC) similar to the Apollo reentry module. Both vehicles used only RCS thrusters for attitude control, however the aerodynamic characteristics are drastically different. The techniques presented to control these vehicles during reentry consist of two modules: (i) the attitude controller using the trajectory linearization control (TLC) technique, and (ii) the control allocation module using lookup table based dynamic inversion and dynamic torque matching technique.

Nonlinear tracking and decoupling control by trajectory linearization[1] is one of the advanced nonlinear control techniques that can be viewed as the ideal gain-scheduling controller designed at every point on the flight trajectory. A prototype trajectory linearization controller (TLC) design for the X-33 ascent[2] and entry[3] flight phases was developed under NASA MSFC Advanced Guidance and Control Program and NASA Space Launch Initiative NRA8-30[4,5,6]. For each flight phase, the controller has only 36 tunable gains that remain constant for nominal flight, dispersions and failure conditions. Initial testing of the TLC ascent and entry controllers showed encouraging results. During the 2003 NASA MSFC Integration and Testing of Advanced Guidance and Control (ITAG&C) program[7], the TLC control algorithm was able to fly the most dispersion and failure test cases. In fact, the only test cases that the TLC design could not fly were the cases that no other algorithms could fly at that time.

The TLC employs an open-loop controller that acquires the nominal guidance trajectory, and a closed-loop controller that asymptotically eliminates (stabilizes) the guidance command tracking error due to vehicle and environmental dispersions and vehicle failures. Therefore it provides robust stability and performance at all stages of flight without interpolation of controller gains, thereby eliminating costly controller redesigns due to minor airframe alteration or mission

---

*Graduate Student, School of EECS

†Research Engineer, Avionic Engineering Center

‡Corresponding author, AIAA Member, Professor, School of EECS, zhuj@ohio.edu

§Advanced Space Transportation, Associate Fellow AIAA

reconfiguration. The TLC computes the commanded torque symbolically based on the theoretical derivations, which are applicable to any feasible trajectories and airframes with known mass properties. Therefore the design is vehicle scalable and mission adaptable. In particular, it should be applicable to the WLB and ASC without much alteration.

To examine and demonstrate the vehicle scalability and mission adaptability of the TLC control technique, the TLC control algorithm is applied to both of the aforementioned crew transfer vehicle models in entry flight phases with a set of fixed gains for the nominal flight conditions. The gain parameters along with initial design verification test simulation results are presented in this paper. The verification simulations are performed in IDOS, which is a MATLAB/SIMULINK 6-DOF launch vehicle simulation environment, developed by Universal Space Lines LLC under NRA8-30[8].

Another flight controller design challenge for the crew return vehicles is the control allocation, which realizes the attitude controller's torque command by selecting RCS thrusters, or deflecting aerodynamic control surfaces if they are available. The only available control effectors for the WLB and ASC concept vehicles are RCS thrusters with limited fuel. The discrete-time, discrete-thrust nature of the RCS control not only introduces large errors in the control torque realization, but also introduces high-frequency noises and significant delays in the control loop. These problems will increase guidance command tracking errors and decrease the robustness and stability margin of the attitude control. Further compounding the problem is the sensitivity of the vehicle dynamics and RCS control to the offset of vehicle CG. The large number of attainable control moment (ACM) vectors from all combinations of the RCS thrusters, while providing redundancies in case of RCS failures, renders control allocation by enumeration of the ACM vectors impractical.

A lookup table algorithm is presented to compress the large amount of ACM vector data into a format which can be used to quickly generate a set of RCS thruster commands to closely match a commanded vehicle body torque. Common practices in control allocation[9,10] seek to map instantaneous torque commands to the vehicle control surfaces and/or RCS thrusters. An alternative approach is a dynamic allocation where the torque is allocated by matching a commanded torque over a past time interval, or matching a torque impulse. In addition, the RCS actuator dynamics will be accounted for by a dynamic pseudo-inverse. Preliminary control allocation results are included in this paper.

Following this introduction, Section 2 presents an overview of the generalized TLC control method applicable to reentry space vehicles. The table lookup control allocation method is presented in Section 3. Preliminary simulation and verification results from IDOS are presented in Section 4. Section 5 concludes the paper with a summary of the main results and issues that need to be addressed by further research..

## 2. Trajectory Linearization Attitude Controller

Consider output tracking by a nonlinear dynamic system

$$\begin{aligned}\dot{\xi}(t) &= f(\xi(t), \mu(t), \theta(t)) \\ \eta(t) &= h(\xi(t), \mu(t), \theta(t))\end{aligned} \tag{1}$$

Where $\xi(t)$ denotes the state trajectory, $\eta(t)$ the output trajectory, $\mu(t)$ the control input, and $\theta(t)$ time dependent parameters. Let $\bar{\xi}(t), \bar{\eta}(t), \bar{\mu}(t)$ be the nominal state, output trajectories and nominal control satisfying

$$\begin{aligned}\dot{\bar{\xi}}(t) &= f(\bar{\xi}(t), \bar{\mu}(t), \theta(t)) \\ \bar{\eta}(t) &= h(\bar{\xi}(t), \bar{\mu}(t), \theta(t))\end{aligned}$$

Define the state and output tracking errors, and the tracking error control input by

$$\begin{aligned}\tilde{\xi}(t) &= \xi(t) - \bar{\xi}(t) \\ \tilde{\eta}(t) &= \eta(t) - \bar{\eta}(t) \\ \tilde{\mu}(t) &= \mu(t) - \bar{\mu}(t)\end{aligned}$$

The nonlinear tracking error dynamics can then be written as

$$\begin{aligned}\dot{\tilde{\xi}}(t) &= f\left(\bar{\xi}(t) + \tilde{\xi}(t), \bar{\mu}(t) + \tilde{\mu}(t), \theta(t)\right) \\ &\quad - f\left(\bar{\xi}(t), \bar{\mu}(t), \theta(t)\right) \\ &= F\left(\tilde{\xi}(t), \tilde{\mu}(t), \theta(t), \bar{\xi}(t), \bar{\mu}(t)\right) \\ \tilde{\eta}(t) &= h\left(\bar{\xi}(t) + \tilde{\xi}(t), \bar{\mu}(t) + \tilde{\mu}(t), \theta(t)\right) \\ &\quad - h\left(\bar{\xi}(t), \bar{\mu}(t), \theta(t)\right) \\ &= H\left(\tilde{\xi}(t), \tilde{\mu}(t), \theta(t), \bar{\xi}(t), \bar{\mu}(t)\right)\end{aligned}$$

Asymptotic tracking can then be achieved by a 2 Degrees-of-Freedom (DOF) controller consisting of: (i) a dynamic inverse I/O mapping $\eta \mapsto \mu$ of the plant to compute the nominal control $\bar{\mu}(t)$ for any given nominal output trajectory $\bar{\eta}(t)$, and (ii) a tracking error stabilizing control law $\tilde{\mu}$ to account for modeling uncertainties, disturbances and initial conditions.The overall controller configuration is given in Figure 1.

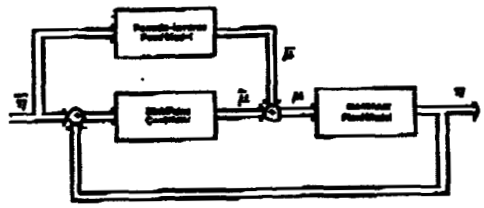

Figure 1. Nonlinear Tracking System Configuration

The trajectory linearization tracking controller uses a linear time-varying (LTV) stabilization controller to stabilize the nominal (command) trajectory $\bar{\eta}$ with a linear state feedback control law $\tilde{\mu} = K(t)\tilde{\xi}(t)$. For the WLB and ASC flight controllers, the LTV control law will be computed using parallel-differential (PD)-eigenstructure assignment. A detailed theoretical background on nonlinear inversion and PD-eigenstructure is given in[1]. To make this paper self-contained, the main design results are summarized below.

State variables of the WLB and ASC attitude equations of motion in entry and launch abort flight are the acrodynamic angle vector $\eta$ and body rate vector $\omega$; and the control input is the body torque vector $T$, which are given, respectively, by

$$\eta = \begin{bmatrix} \varphi \\ \alpha \\ \beta \end{bmatrix}, \qquad \omega = \begin{bmatrix} p \\ q \\ r \end{bmatrix}, \qquad T = \begin{bmatrix} T_l \\ T_m \\ T_n \end{bmatrix}$$

where $\varphi$, $\alpha$, and $\beta$ are the bank, angle of attack, and sideslip angles; $p$, $q$, and $r$ are the roll, pitch, and yaw rates; and $T_l$, $T_m$, $T_n$ are the roll, pitch and yaw moments about the vehicle center of gravity due to airframe and control surface aerodynamics, and RCS thrusts. The kinematic equations $\dot{\eta} = f_\eta(\eta, \omega)$ are given by:

$$\begin{aligned} \dot{\varphi} &= [p\cos(\alpha) + r\sin(\alpha)]/\cos(\beta) + \dot{\chi}\sin(\vartheta) \\ &\quad - \tan(\beta)[\cos(\vartheta)\cos(\varphi) - Z_{accel}]G/V \\ \dot{\alpha} &= q - \tan(\beta)[p\cos(\alpha) + r\sin(\alpha)] \\ &\quad + [\cos(\vartheta)\cos(\varphi) - Z_{accel}]G/V/\cos(\beta) \\ \dot{\beta} &= p\sin(\alpha) - r\cos(\alpha) \\ &\quad + [\cos(\vartheta)\sin(\varphi) - Y_{accel}]G/V \end{aligned} \tag{2}$$

where $\chi$ is the heading angle, $\vartheta$ is the flight path angle, $V$ is the magnitude of the relative velocity, $G$ is the gravitational constant, $Y_{accel}$ and $Z_{accel}$ are the lateral and normal accelerations in the Wind Frame, respectively. The body rate dynamic equations $\dot{\omega} = f_\omega[\omega, J, J^{-1}]$:

$$\begin{aligned} \dot{p} &= I^p_{pq}pq + I^p_{qr}qr + g^p_l\left(C_{N_p}p + C_{N_r}r + T_l\right) \\ &\quad + g^p_n\left(C_{N_p}p + C_{N_r}r + T_n\right) \\ \dot{q} &= I^q_{pp}p^2 + I^q_{rr}r^2 + I^q_{pr}pr + g^q_m\left(C_{M_q}q + T_m\right) \\ \dot{r} &= I^r_{pq}pq + I^r_{qr}qr + g^r_l\left(C_{L_p}p + C_{L_r}r + T_l\right) \\ &\quad + g^r_n\left(C_{N_p}p + C_{N_r}r + T_n\right) \end{aligned} \tag{3}$$

where $I^n_{pq}$, $g^n_l$, etc. are coefficients consisting of the moments of inertia;

$$C_{L_p} = \frac{\partial L}{\partial p}, \qquad C_{L_r} = \frac{\partial L}{\partial r}$$

$$C_{M_q} = \frac{\partial M}{\partial q}$$

$$C_{N_p} = \frac{\partial N}{\partial p}, \qquad C_{N_r} = \frac{\partial N}{\partial r}$$

are the dynamic derivatives, and $J$ is the inertia matrix

$$J = \begin{bmatrix} I_{xx} & 0 & -I_{xz} \\ 0 & I_{yy} & 0 \\ -I_{xz} & 0 & I_{zz} \end{bmatrix}$$

Owing to the block-triangular form of the equations of motion(2) and (3), the plant admits an inner-outer loop controller design which greatly simplifies the PD-eigenvalue assignment and the nonlinear dynamic inversion. However, the validity of this design rests on the requirement that the inner loop dynamics must be sufficiently fast so as to render it as a singular perturbation to the outer loop. The trajectory linearization controller configuration shown in Figure 1 is applied to both the attitude error feedback loop and angular rate error feedback loop.

For attitude angle tracking, the nominal body rate $\bar{\omega} = [\bar{p} \quad \bar{q} \quad \bar{r}]^T$ is given by

$$\begin{aligned} \bar{p} &= \dot{\bar{\varphi}}\cos(\bar{\alpha}) - [\sin(\bar{\varphi}) - Y_{accel}]\sin(\bar{\alpha})G/V \\ &\quad - \dot{\chi}\sin(\vartheta)\cos(\bar{\alpha}) \\ \bar{q} &= \dot{\bar{\alpha}} - (\cos(\bar{\varphi}) - Z_{accel})G/V \\ \bar{r} &= \dot{\bar{\varphi}}\sin(\bar{\alpha}) + [\sin(\bar{\varphi}) - Y_{accel}]\cos(\bar{\alpha})G/V \\ &\quad - \dot{\chi}\sin(\vartheta)\sin(\bar{\alpha}) \end{aligned} \tag{4}$$

For body rate tracking, the nominal body torque $\bar{T} = [\bar{T}_l \quad \bar{T}_m \quad \bar{T}_n]^T$, assuming $I_{xy} = I_{yz} = 0$, is given by

$$\begin{aligned}\overline{T}_l &= I_{xx}\dot{\overline{p}} + (I_{zz} - I_{yy})\overline{q}\,\overline{r} \\ &\quad - I_{xz}(\dot{\overline{r}} + \overline{q}\,\overline{p}) - C_{L_p}\overline{p} - C_{L_r}\overline{r} \\ \overline{T}_m &= I_{yy}\dot{\overline{q}} + (I_{zz} - I_{xx})\overline{p}\,\overline{r} \\ &\quad + I_{xz}(\overline{p}^2 - \overline{r}^2) - C_{M_q}\overline{q} \\ \overline{T}_n &= I_{zz}\dot{\overline{r}} + (I_{yy} - I_{xx})\overline{q}\,\overline{p} \\ &\quad + I_{xz}(\overline{q}\,\overline{r} - \dot{\overline{p}}) - C_{N_p}\overline{p} - C_{N_r}\overline{r}\end{aligned} \tag{5}$$

Integral feedback is employed for disturbance accommodation and robustness to parametric uncertainties. The attitude and rate tracking error state variables are defined, respectively, by

$$\eta_{\text{aug}} = \begin{bmatrix} \int(\varphi - \varphi_{\text{com}})dt \\ \varphi - \varphi_{\text{com}} \\ \int(\alpha - \alpha_{\text{com}})dt \\ \alpha - \alpha_{\text{com}} \\ \int(\beta - \beta_{\text{com}})dt \\ \beta - \beta_{\text{com}} \end{bmatrix}, \quad \omega_{\text{aug}} = \begin{bmatrix} \int(p - p_{\text{com}})dt \\ p - p_{\text{com}} \\ \int(q - q_{\text{com}})dt \\ q - q_{\text{com}} \\ \int(r - r_{\text{com}})dt \\ r - r_{\text{com}} \end{bmatrix}$$

where commanded bank angle, $\varphi_{\text{com}}$ and commanded angle of attack, $\alpha_{\text{com}}$ are given by the closed-loop entry guidance, and the sideslip angle $\beta_{\text{com}} \equiv 0°$ must be tightly regulated. The proportional-integral (PI) feedback control law for the attitude loop tracking error is given by $u_1 = -K_1(t)\eta_{\text{aug}}$, where the gain matrix $K_1(t)$ is computed symbolically as

$$K_1(t) = \begin{bmatrix} k_{111} & k_{112} & 0 & \overline{r} & k_{115} & k_{116} \\ 0 & k_{122} & \alpha_{121} & \alpha_{122} & 0 & k_{126} \\ k_{131} & k_{132} & 0 & -\overline{p} & k_{135} & k_{136} \end{bmatrix} \tag{6}$$

where

$$\begin{aligned} k_{111} &= \cos(\overline{\alpha})\,\alpha_{111} \\ k_{112} &= \cos(\overline{\alpha})\,\alpha_{112} + \sin(\overline{\alpha})\cos(\overline{\varphi})G/V \\ k_{115} &= \sin(\overline{\alpha})\,\alpha_{131} \\ k_{116} &= \sin(\overline{\alpha})\,\alpha_{132} \\ &\quad - (\cos(\overline{\varphi}) - Z_{\text{accel}})\cos(\overline{\alpha})G/V \\ k_{122} &= -\sin(\overline{\varphi})G/V \\ k_{126} &= -[\overline{p}\cos(\overline{\alpha}) + \overline{r}\sin(\overline{\alpha})] \\ k_{131} &= \sin(\overline{\alpha})\,\alpha_{111} \\ k_{132} &= \sin(\overline{\alpha})\,\alpha_{112} - \cos(\overline{\alpha})\cos(\overline{\varphi})G/V \\ k_{135} &= -\cos(\overline{\alpha})\,\alpha_{131} \\ k_{136} &= -\cos(\overline{\alpha})\,\alpha_{132} \\ &\quad - [\cos(\overline{\varphi}) - Z_{\text{accel}}]\sin(\overline{\alpha})G/V \end{aligned}$$

Similarly, the PI feedback control law for the rate loop tracking error is given by $u_2 = -K_2(t)\omega_{\text{aug}}$. The gain matrix $K_2(t)$ is computed symbolically by

$$K_2(t) = \begin{bmatrix} k_{211} & k_{212} & 0 & k_{214} & k_{215} & k_{216} \\ 0 & k_{222} & k_{223} & k_{224} & 0 & k_{226} \\ k_{131} & k_{132} & 0 & k_{234} & k_{236} & k_{236} \end{bmatrix} \tag{7}$$

where

$$\begin{aligned} k_{211} &= I_{xx}\,\alpha_{211} \\ k_{212} &= I_{xz}(I^p_{pq}\overline{q} + \alpha_{212}) - I_{xz}I^r_{pq}\overline{q} + C_{L_p} \\ k_{214} &= I_{xz}(I^p_{pq}\overline{p} + I^p_{qr}\overline{r}) - I_{xz}(I^r_{pq}\overline{p} + I^r_{qr}\overline{r}) \\ k_{215} &= -I_{xz}\,\alpha_{231} \\ k_{216} &= I_{xz}I^p_{qr}\overline{q} - I_{xz}(I^r_{qr}\overline{q} + \alpha_{232}) + C_{L_r} \\ k_{222} &= I_{yy}(2I^q_{pp}\overline{p} + I^q_{pr}\overline{r}) \\ k_{223} &= I_{yy}\,\alpha_{221} \\ k_{224} &= C_{M_q} + I_{yy}\alpha_{222} \\ k_{226} &= I_{yy}(2I^q_{rr}\overline{r} + I^q_{pr}\overline{p}) \\ k_{231} &= -I_{xz}\,\alpha_{211} \\ k_{232} &= I_{xz}I^r_{pq}\overline{q} - I_{xz}(I^p_{pq}\overline{q} + \alpha_{212}) + C_{N_p} \\ k_{234} &= I_{xz}(I^r_{pq}\overline{p} + I^r_{qr}\overline{r}) - I_{xz}(I^p_{pq}\overline{p} + I^p_{qr}\overline{r}) \\ k_{235} &= I_{xz}\,\alpha_{231} \\ k_{236} &= I_{xz}(I^r_{qr}\overline{q} + \alpha_{232}) - I_{xz}I^p_{qr}\overline{q} + C_{N_r} \end{aligned}$$

In the above gain matrices $K_1(t)$ and $K_2(t)$, the parameters $\alpha_{ijl}(t)$, $i = 1,2$, $j = 1,2,3$, $l = 1,2$ are obtained from the closed-loop quadratic PD-eigenvalues

$$\rho_{ijl}(t) = -\left(\zeta_{ij} \pm \sqrt{1 - \zeta_{ij}^2}\right)\omega^2_{nij}(t) \tag{8}$$

for $\zeta_{ij} \neq 1$, with constant damping $\zeta_{ij}$ and time-varying bandwidth $\omega_{nij}(t)$ as follows

$$\begin{aligned} \alpha_{ij1}(t) &= \omega^2_{nij}(t) \\ \alpha_{ij2}(t) &= 2\zeta_{ij}\omega_{nij}(t) - \frac{\dot{\omega}_{nij}(t)}{\omega_{nij}(t)} \end{aligned} \tag{9}$$

Closed-loop stability with respect to the equations of motion is established for $\zeta_{ij} > 0$ and $\omega_{nij}(t) > 0$, for all $t > 0$. As a constraint of the singular perturbation method, the inner loop bandwidth $\omega_{n2j}(t)$ must be sufficiently greater than the outer-loop bandwidth $\omega_{n1j}(t)$ to ensure stability. In addition, $\zeta_{ij} = 1.0$ should be avoided. The time-varying bandwidth $\omega_{n1j}(t)$ can be used for adaptation to vehicle and environmental dispersions and control effector failures.

The reference signal for the outer loop is the commanded attitude $\eta_{\text{com}} = \overline{\eta}$. The inner loop reference is the commanded body rate $\omega_{\text{com}} = \overline{\omega} + u_1$. The controller output is the commanded torque $T_{\text{com}} = \overline{T} + u_2$, which is the input to the control allocation unit. The commanded torque is realized via

the neural network based control allocation unit discussed in the following section.

Due to the integral (high-gain) control, loss of control authority due to excessive disturbances such as wind gust, vehicle dispersions such as overly estimated control effectiveness, and control effector failure such as loss of one or more RCS thrusters, will result in torque command saturation. This in effect increases the level of singular perturbations to the outer control loops, which may result in performance degradation or even loss of stability. By the singular perturbation theory, reducing the outer loop bandwidth accordingly can ensure stability and performance, although the overall response time will be longer. The time-varying bandwidth capability of the PD-eigenvalue assignment technique allows the vehicle to adapt to severe dispersions and partial control effector failures without explicit fault identification. This is known as direct fault tolerant control, and has been demonstrated to be very effective under the NRA8-30 Program[11].

The overall flight controller consists of 6 PI controllers, one for each channel in the inner and outer loops (note that the outer loop is effectively controlled by a proportional-integral-derivative (PID) controller, as the inner loop serves as a derivative feedback). Each channel has a nominal controller containing a pseudo-differentiator. With a constant rate time-varying bandwidth $\omega_{ni,j}(t)$, each channel in a loop has 6 constant design parameters to be tuned for stability and performance. The total number of tunable design parameters is 36, which include: $\omega_{n1k,\text{diff}}, k=1,2,3$, which are the bandwidth of the outer loop pseudo-differentiator for the roll, pitch and yaw channel, respectively; $\zeta_{1k}$, which is the damping ratio and $\omega_{n1k,\min}$, $\omega_{n1k,\max}$ which are the lower and upper limits of the closed-loop bandwidth for the attitude error dynamics; $\omega_{n1k,\text{dec}}$ and $\omega_{n1k,\text{inc}}$ which are the decrement and increment of the outer loop bandwidth per control cycle when any of the control moment command exceeds or recedes the maximum attainable moment in that channel (torque command saturation), respectively. The inner loop counterparts $\omega_{n2k,\text{diff}}$, $\zeta_{2k}$, $\omega_{n2k,\min}$, $\omega_{n2k,\max}$, $\omega_{n2k,\text{dec}}$ and $\omega_{n2k,\text{inc}}$, $k=1,2,3$, are defined similarly. These constant design parameters, once tuned, are used for all nominal and abort flight conditions without alteration.

## 3. Control Allocation Design

The commanded torque $T_{\text{com}}$ generated by the trajectory linearization attitude controller is realized via a control allocation unit that produces the corresponding RCS firing command $\delta$, which is an $N$-dimensional, binary-valued vector, where $N$ is the number of thrusters, the $i$th entry $\delta_i$ corresponds to the $i$th thruster's on-off command with $\delta_i = 1$ for thruster on, and $\delta_i = 0$ thruster off. It is a common practice to formulate the control allocation problem as finding a $\delta$ such that

$$T = B\delta = T_{\text{com}} \tag{10}$$

where $B$ is the thrust-to-moment table for all RCS thrusters, or the control effectiveness matrix, which can be obtained from a given vehicle RCS configuration. The control allocation, or the RCS thruster selection logic design thus amounts to finding an inverse mapping $T_{\text{com}} \rightarrow \delta$.

The WLB and the ASC both employ only RCS control effectors. For a vehicle configuration with $N$ RCS thrusters, the total number of attainable control moments is $2^N$, which constitutes the attainable moment set in the roll-pitch-yaw moment space. To ensure effective attitude control and guidance command tracking, and to minimize RCS fuel consumption, it is desirable that the attainable moments be distributed evenly in the moment space.

The range of moments attainable from the 16 RCS thrusters on the WLB are shown in figures 2-4, the moment range attainable from the 12 thrusters on the ASC are shown in figures 5-7. These figures show the entire set of attainable moments in each channel from least to greatest magnitude. The segments with gaps between adjacent points on the lines indicate unattainable moments within the range. The roll moment sets for both configurations indicate a number of roll moments that are unattainable by any combination of thruster firings. The ASC has particularly uneven roll moment distribution, which greatly reduces the controllability of the vehicle.

The distribution of moments in one channel with respect to another channel is important in determining the ability of a control allocation algorithm to meet a large combination of commanded roll, pitch, and yaw moments. The distribution of moments in the moment space are shown in figures 8-10 the WLB, and figures 11-13 for the ASC. A dense, even distribution such as the pitch vs. yaw moment plot for the WLB in figure 10 is desirable because it indicates that almost any combination of pitch and yaw moments can be realized. On the other hand, a distribution such as the roll vs. yaw plot in figure 12 for the ASC indicates that for any desired yaw moment, there are few corresponding roll moments, which also reduces the controllability of the vehicle about the roll axis.

It is noted that at high angles of attack, both sideslip regulation and bank command tracking require

coordinated roll-yaw control. Thus the attainable stability margin and guidance command tracking performance can be improved significantly if the orientation and location of the thrusters can be adjusted within the vehicle configuration constraints so as to improve the distribution of the attainable roll-yaw moments. In fact, the distribution of attainable moments from a thruster configuration can be significantly improved by making slight adjustments in the plume directions of a few thrusters. Given the impact of moment distributions on the controllability of a vehicle, it would be prudent to address this issue early in the vehicle design stage.

Due to the binary-valued RCS control effector vector $\delta$, the inverse mapping cannot be constructed using a pseudo-inverse of the $B$ matrix in equation (10). Thruster allocation by table lookup is a simple algorithm capable of finding a set of RCS thruster commands that produces a body torque which closely matches the commanded torque. The lookup table method is the most accurate way to allocate control to the RCS thrusters during nominal flight. Since the majority of the computations are done off-line, the lookup table can be configured to trade off accuracy for other considerations such as computational power, memory limitations, fuel consumption, etc. The drawback is that in order to accommodate off-nominal events such as thruster failures, a different lookup table would be needed for each event, which may not be feasible with limited onboard computational resources.

The lookup table is constructed by first discretize the range of attainable control moments along the roll, pitch, and yaw axes with a desired resolution. The discretized moment values along each axis are ordered monotonically increasing to produce a roll, pitch, and yaw moment analog-to-digital conversion (ADC) vector, respectively, so that each discrete interval along the roll, pitch, and yaw moment axes can be indexed with an integer, and each discrete (rectangular) cell in the attainable moment set can be indexed with a 3-dimensional index vector that serves as the indices for the lookup table.

Each attainable moment is represented by an $N$-digit binary number corresponding to the RCS thruster firing combination $\delta$. The lookup table is then constructed by choosing one attainable moment from each cell. Each cell of the table is thus filled with an integer corresponding to the binary number. If there are more than one attainable moment in a cell, the one that uses the least number of thrusters will be chosen. If a cell is empty, then an attainable moment from a nearby cell that is in a certain sense closest will be chosen.

A trade off between accuracy and computational constraints can be met by adjusting the resolution at which the moment ranges are discretized. Since the discretized ADC vectors need not be the same length, a certain channel may be favored by discretizing the moment set of that channel at a higher resolution. The method of determining the closest cell to an empty cell can also be tailored to favor a certain channel by only searching along the other two axes. A logic algorithm could produce one of several tables with different performance characteristics based on current vehicle conditions.

Lookup tables were created for the WLB and ASC thruster configurations. The tables for both used 60 partitions along each axis which resulted in lookup tables with $60^3$ elements. The lookup tables were then used to find thruster commands to meet the torque commands from a typical entry torque command profile. The body torque induced by the thruster commands found from the lookup tables are plotted over the commanded torque in figures 14-16 for the WLB, and figures 17-19 for the ASC.

## 4. Simulation Test Results

At this time, preliminary test results for the TLC controller are shown in Figures 20-31. The test simulations were performed in IDOS, which is a MATLAB/SIMULINK 6-DOF launch vehicle simulation environment. Figures 20-22 and 27-28 show outer-loop tracking performance for the WLB and ASC, respectively. Figures 26-28 and 29-31 show inner-loop tracking performance for the WLB and ASC, respectively. Although the two vehicle models differ drastically, in these initial tests the TLC controllers for these two vehicles used the same gains. While further tuning with increased fidelity of the models will likely lead to different gains, the current results have demonstrated the vehicle scalability and mission adaptability of the TLC control technique.

## 5. Summary and Conclusions

In this paper we have demonstrated the vehicle scalability and mission adaptability of the trajectory linearization control (TLC) technique by applying it to the design of entry flight controllers for two drastically different small reentry vehicle—a winged lifting body configuration and an axial-symmetric capsule configuration. Initial test results showed satisfactory performance with the same constant controller gains. Moreover, each flight controller only uses 18 constant controller gains when no adaptation is employed, and with 36 constant controller gains direct fault tolerance adaptation can be implemented.

In addition to the TLC attitude controller, a table-look up RCS control allocation design method is presented. The method is simple yet effective, as has been demonstrated with preliminary test results. The design presented herein is only the first step of a dynamic control allocation technique. Additional work is being performed to implement the dynamic table-lookup method which provides best match of the commanded torque over a recent past interval of time, rather than the matching the instantaneous torque command.

## Acknowledgment

This work has been supported in part by the NASA contract NAS8-01098.

## References

[1] J. Zhu, "Nonlinear Tracking and Decoupling by Trajectory Linearization", Lecture Note, Presented at NASA Marshall Space Flight Center, 137 pp., June 1998.

[2] J. Zhu, B. D. Banker and C. E. Hall, "X-33 ascent flight controller design by trajectory linearization — a singular perturbational approach," AIAA-2000-4159, Proc., AIAA GNC Conference, Denver, CO, Aug. 2000..

[3] J. Zhu, A. S. Hodel, K. Funston and C. E. Hall, "X-33 entry flight controller design by trajectory linearization - a singular perturbational approach," Proc. American Astro. Soc. G&C Conf., Breckenridge, CO, pp. 151-170, Jan. 2001.

[4] John M. Hanson, "Advanced Guidance and Control Project for Reusable Launch Vehicles," AIAA-2000-3957, Proc. AIAA GNC Conference, Denver, CO, Aug. 2000.

[5] Hanson, J., "A Plan for Advanced Guidance and Control Technology for 2nd Generation Reusable Launch Vehicles," AIAA-2002-4557, Proc. AIAA GNC Conf., Monterey CA, Aug. 2002.

[6] Hanson, J., "Advanced Guidance And Control Methods for Reusable Launch Vehicles: Test Results," AIAA-2002-4561, Proc. AIAA GNC Conf., Monterey CA, Aug. 2002.

[7] Hanson, J., "Integration and Testing of Advanced Guidance and Control Technologies," AG&C Workshop, NASA/MSFC, July, 2003.

[8] Joseph E. Fisher, Tim Bevacqua, Douglas A. Lawrence and J. Jim Zhu, "Integrated G&C Implementation within IDOS - A Simulink Based Reusable Launch Vehicle Simulation," AIAA-2003-5496, Proc. AIAA GNC Conf., Austin, TX, August, 2003.

[9] A. Scottedward Hodel, "Convex Programming in the Design of a Control System for a Reusable Launch Vehicle," Proc. AIAA GNC Conf., Denver, CO, Aug. 2000.

[10] A. Scotteward Hodel and Ronnie Callahan, "Autonomous Reconfigurable Control Allocation (ARCA) for Reusable Launch Vehicles", AIAA-2002-4777, Proc. AIAA GNC Conf., Monterey, CA, Aug. 2002.

[11] J. Zhu, D. A. Lawrence, J. Fisher, Y. Shtessel, A. S. Hodel, P. Lu, "Direct Fault Tolerant RLV Attitude Control - A Singular Perturbation Approach," AIAA-2002-4778, Proc., AIAA GNC Conf., Monterey, CA; Aug. 2002.

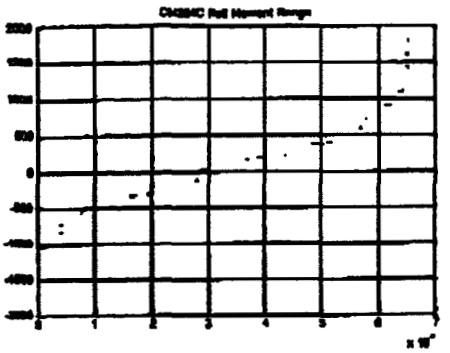

Figure 2 - WLB roll moment range

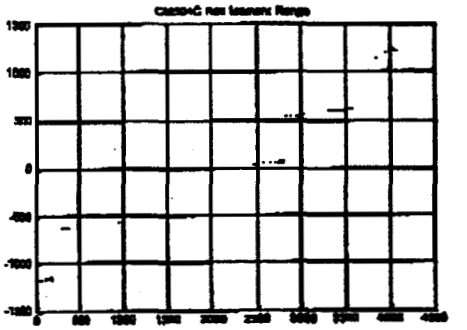

Figure 5 - ASC roll moment range

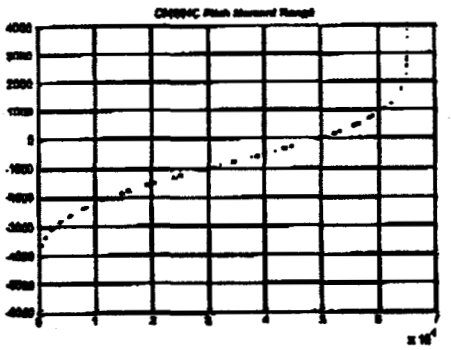

Figure 3 - WLB pitch moment range

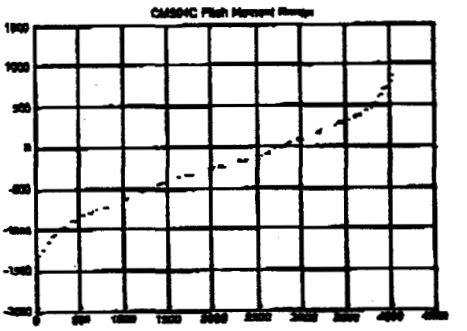

Figure 6 - ASC pitch moment range

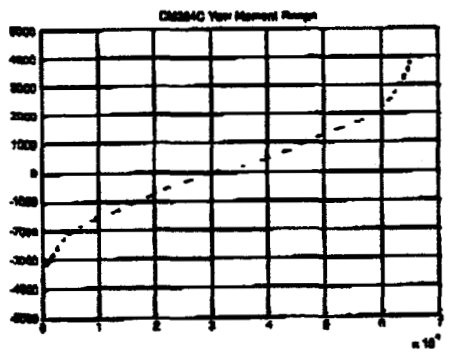

Figure 4 - WLB yaw moment range

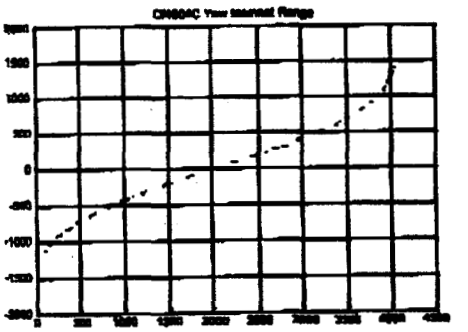

Figure 7 - ASC yaw moment range

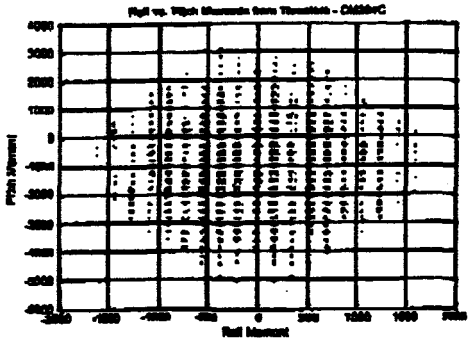

Figure 8 - WLB roll vs. pitch moments

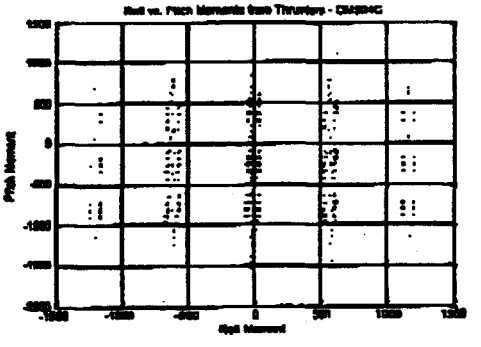

Figure 11 - ASC roll vs. pitch moments

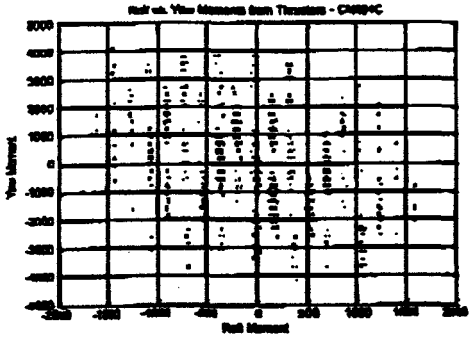

Figure 9 - WLB roll vs. yaw moments

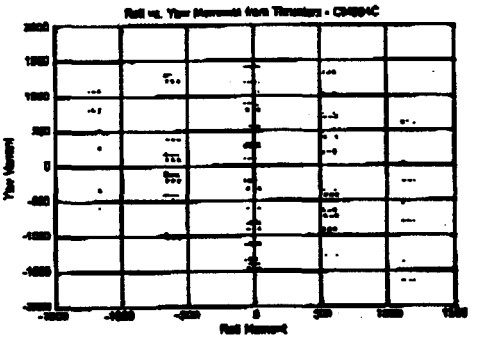

Figure 12 - ASC roll vs. yaw moments

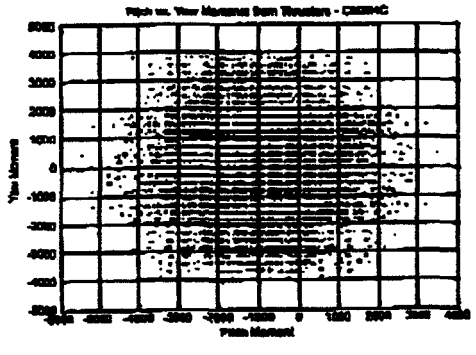

Figure 10 - WLB pitch vs. yaw moments

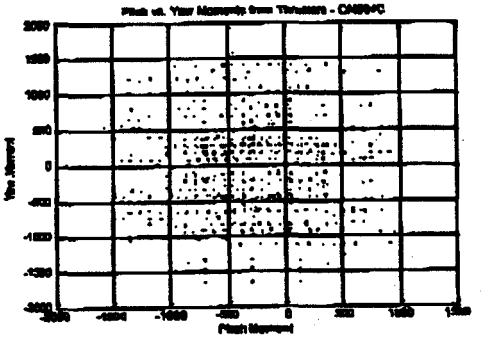

Figure 13 -ASC pitch vs. yaw moments

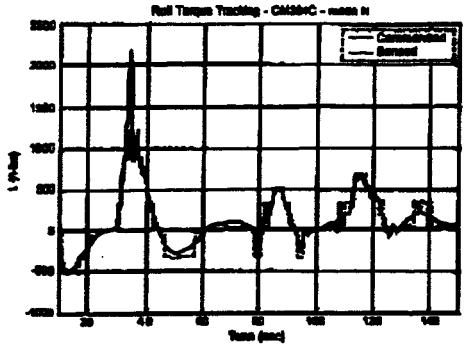

Figure 14 - WLB roll moment tracking

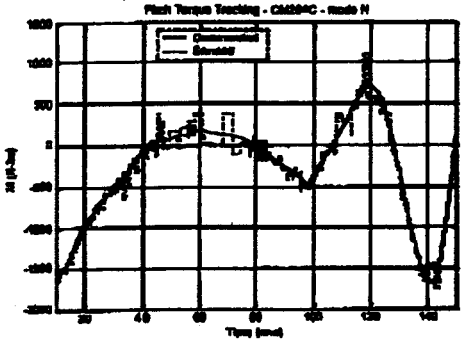

Figure 15 - WLB pitch moment tracking

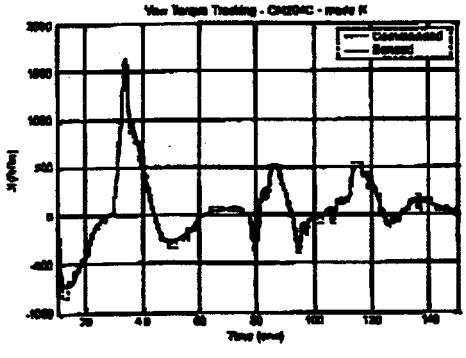

Figure 16 - WLB yaw moment tracking

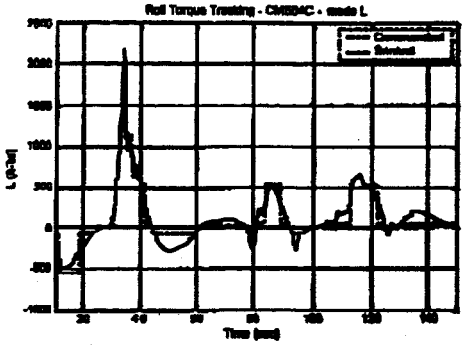

Figure 17 - ASC roll moment tracking

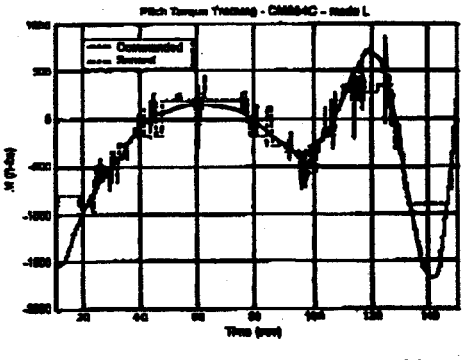

Figure 18 - ASC pitch moment tracking

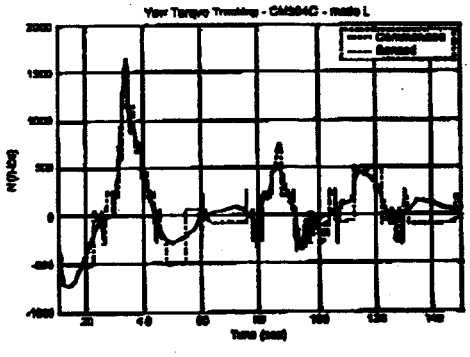

Figure 19 - ASC yaw moment tracking

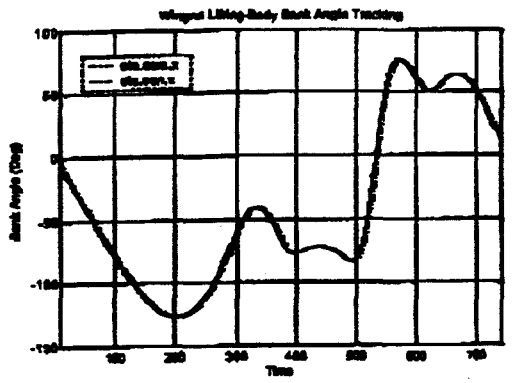

Figure 20 - WLB bank angle tracking

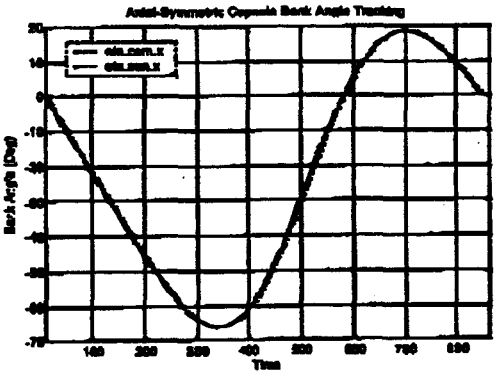

Figure 23 - ASC bank angle tracking

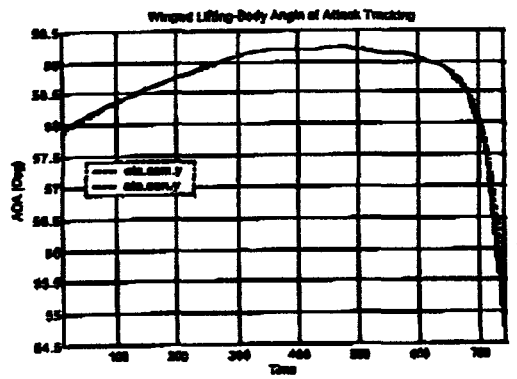

Figure 21 - WLB angle of attack tracking

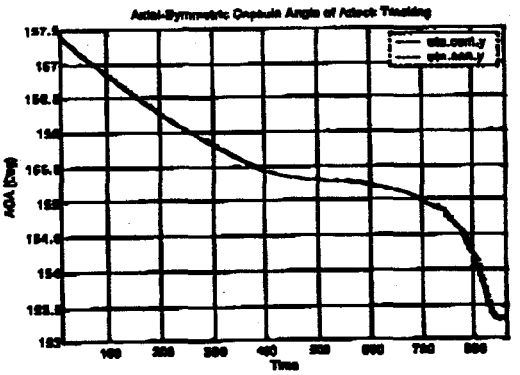

Figure 24 - ASC angle of attack tracking

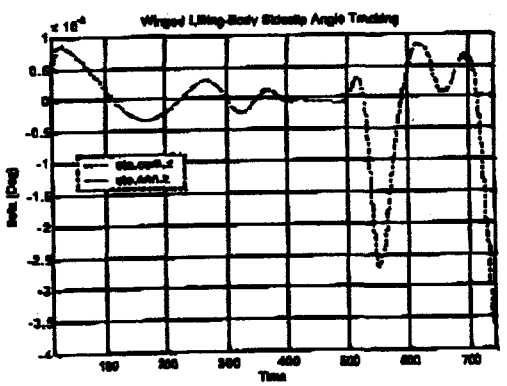

Figure 22 - WLB sideslip angle tracking

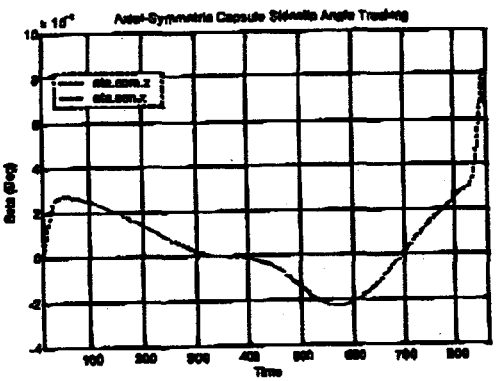

Figure 25 - ASC sideslip angle tracking

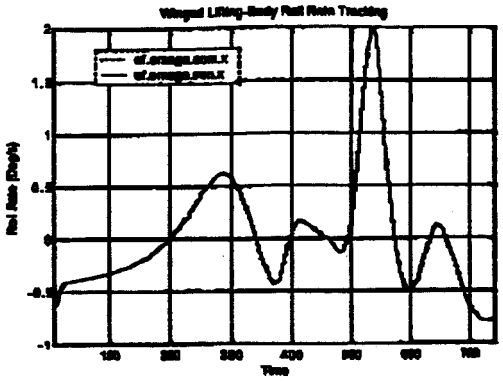

Figure 26 - WLB roll rate tracking

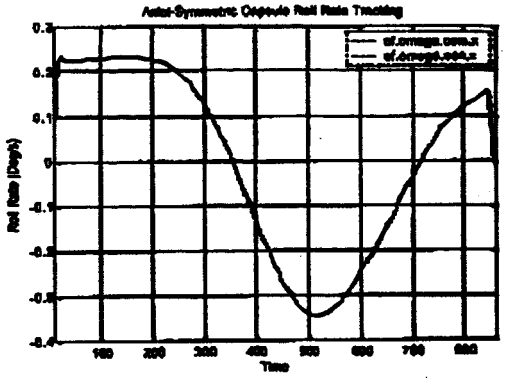

Figure 29 - ASC roll rate tracking

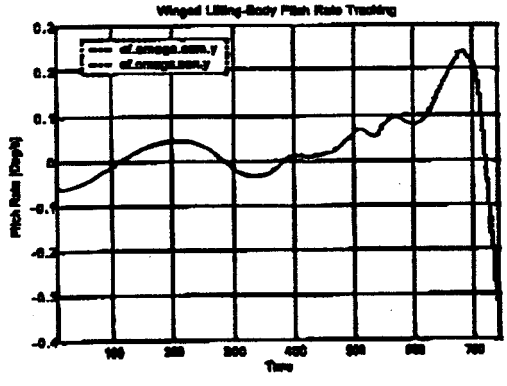

Figure 27 - WLB pitch rate tracking

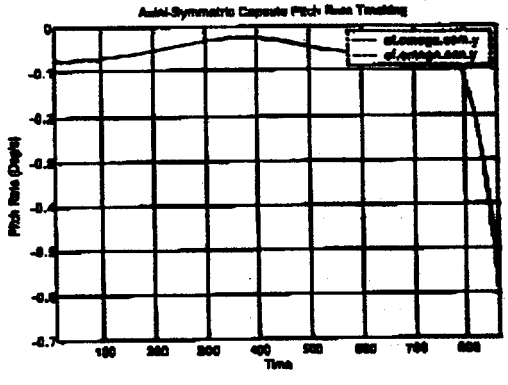

Figure 30 - ASC pitch rate tracking

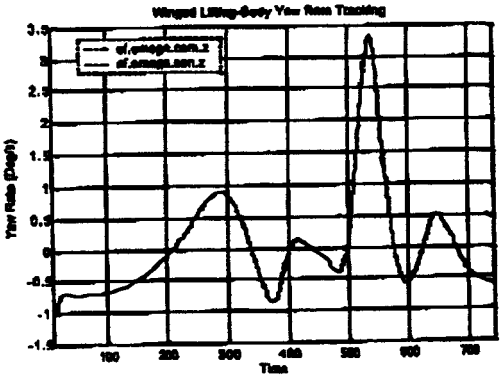

Figure 28 - WLB yaw rate tracking

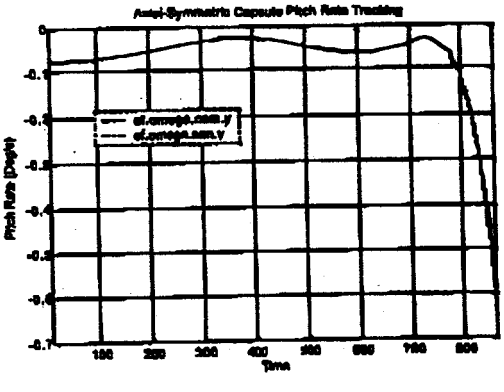

Figure 31 - ASC yaw rate tracking

Jack Mu
Bldg. 420

National Aeronautics and Space Administration

# Routing Slip

| | Mail Code | Name | Action | |
|---|---|---|---|---|
| | | | Approval | |
| 1 | UP20 | Bob Armstrong | Call me | |
| | | | Concurrence | |
| 2 | UP30 | M. Fisher | File | |
| | | | Information | |
| 3 | UP20 | Stephan Davis | Investigate and Advise | |
| | | | Note and Forward | |
| 4 | UP01 | Dennis Smith | Note and Return | |
| | | | Per Request | |
| 5 | AD34 | Betty Fowler | Per Phone Conversation | |
| | | | Recommendation | |
| 6 | | | See me | |
| | | | Signature | |
| 7 | | | Circulate and Destroy | |
| | | | | |

NPG 2200.2A requires a NASA Form 1676 be completed on all documents being published or presented.

As the COTR, please complete this form in Part II, III & VI, then forward to UP30/M. Fisher for Part VII, to UP20/S. Davis for Part VIII & to UP01/D. Smith for Part IX. Please return the 1676 package to AD34 when all Parts have been completed and signed.

Please note the flow diagram added to the latest revision of MPG 2220.1 for guidance & phone me also with any questions.

| Name | Tel. No. *(or Code)* & Ext. |
|---|---|
| Alisha Simmons for Betty Fowler AS | 4-3124 |
| Code *(or other designation)* | Date |
| AD34 | February 18, 2004 |

NASA FORM 26 SEP 96 PREVIOUS EDITIONS ARE OBSOLETE.